Dalton Transactions

ROYAL SOCIETY OF CHEMISTRY

PAPER

View Article Online
View Journal | View Issue

Cite this: *Dalton Trans.*, 2026, **55**, 4119

Sulfur insertion into group 12 metal dithiolate complexes: metal-dependent equilibria

Muhammad Sohail, Carsten Heinsen, Allen G. Oliver and Emily Y. Tsui *

Received 11th January 2026,
Accepted 6th February 2026

DOI: 10.1039/d6dt00074f

rsc.li/dalton

Dianionic bis(carboxamide)pyridine-supported metal(II) dithiolate complexes of Cd^{2+} and Hg^{2+} showed isostructural $[N_3S_2]$ coordination to a previously reported zinc variant, but changes in ionic radius resulted in distortion of the coordination geometries. While addition of elemental sulfur to the zinc dithiolate complex selectively inserts an "S_3" unit to form a zinc tetrasulfanide complex, addition of S_8 to the Cd^{2+} or Hg^{2+} congeners formed multiple products corresponding to sulfur insertion at both thiolate moieties, with different equilibrium constants of insertion. These reactions were correlated to comparisons of metal thiolate nucleophilicity and electrochemical oxidation potentials of the dithiolate complexes. These results point to additional contributions from ring strain and other structural/steric effects in controlling the thermodynamics of sulfur insertion.

Introduction

Thiolate anions react with S_8 to undergo catenation and form polysulfanide anions, a reaction that occurs alongside thiolate oxidation and S_8 reduction to polysulfide anions.[1] This reaction is affected by metal–thiolate interactions. For example, Pluth and co-workers reported that $K(18\text{-c-}6)^+$ cations can selectively stabilize the persulfide anions.[2] Addition of the metal triflate salts of different redox-inactive metal ions (Li^+, Na^+, K^+, Mg^{2+}, Ca^{2+}, Zn^{2+}, Cd^{2+}) to mixtures of arenethiolate anions and sulfur result in divergent metal-dependent speciation.[3] We have previously reported that treatment of a dianionic bis(carboxamide)pyridine-supported zinc dithiolate complex ($[\mathbf{1}\text{-Zn}]^{2-}$, Scheme 1) with elemental sulfur (S_8) selectively inserts three S^0 atom equivalents into a Zn–S(thiolate) bond to form a zinc tetrasulfanide complex ($[\mathbf{2}\text{-Zn}]^{2-}$).[4] It is apparent that chelating thiolate ligands and the resulting ring strain can favor sulfur catenation over thiolate oxidation.[5]

Like Zn^{2+}, the other group 12 divalent ions Cd^{2+} and Hg^{2+} are coordinated strongly by sulfur-containing ligands, including the cysteine residues of the protein metallothionein.[6–8] However, due to differences in the ionic and covalent radii and metal ion polarizability, the thermodynamics of metal–thiolate bonding and thiolate reactivity are expected to vary. For example, complexation studies between these metals and cysteine showed that the formation constants decrease in the order $Hg^{2+} > Cd^{2+} > Zn^{2+}$, an order that is dictated by the metal–sulfur bonding rather than metal–oxygen or metal–nitrogen interactions.[9] The larger metal ions are also known to exhibit relativistic effects, further stabilizing metal–sulfur bonding. These differences in bonding are expected to change the thiolate oxidation potentials, nucleophilicity, and basicity. For these reasons, we were interested in comparing the sulfur insertion reactivity of these metals when coordinated by the same chelating thiolate ligands.

Here, we present the sulfur insertion reactivity of the Cd^{2+} and Hg^{2+} congeners of the dithiolate complex $[\mathbf{1}\text{-Zn}]^{2-}$. These complexes are structurally analogous, with variations in bond lengths and angles due to differences in ionic radii. Increased metal size and stronger metal–thiolate bonding was found to decrease metal thiolate nucleophilicity and shift the thiolate oxidation potentials. While the Cd and Hg congeners also undergo sulfur insertion into the metal–thiolate bonds, the

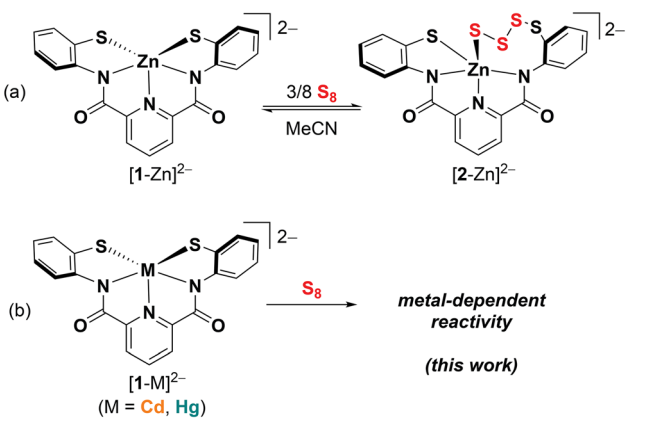

Scheme 1 (a) Formation of a zinc tetrasulfanide complex ($[\mathbf{2}\text{-Zn}]^{2-}$) by sulfur insertion into $[\mathbf{1}\text{-Zn}]^{2-}$. (b) Addition of S_8 to the Cd and Hg congeners of $[\mathbf{1}\text{-Zn}]^{2-}$ show metal-dependent reactivity.

Department of Chemistry and Biochemistry, University of Notre Dame, Notre Dame, Indiana, USA. E-mail: etsui@nd.edu

reactions proceed with lower equilibrium constants and form mixtures of products arising from sulfur insertion at both thiolate moieties. These results show that both the ligand and the metal are critical in determining the outcome of sulfur–thiolate reactivity.

Results and analysis

Synthesis of metal dithiolate complexes

Following a similar procedure for the synthesis of $[Et_4N]_2$[**1**-Zn], the metal dithiolate complexes $[Et_4N]_2$[**1**-M] (M = Cd, Hg) were prepared by deprotonation of the bis(carboxamide)pyridine ligand precursor (H_4L) with sodium bis(trimethylsilyl) amide (NaHMDS, 4 equiv.) and addition of the corresponding metal(II) chloride salt and $[Et_4N]Cl$ (2 equiv.). Fig. 1 shows the solid-state structures of the $[\mathbf{1}\text{-M}]^{2-}$ complexes determined by single crystal X-ray diffraction (XRD). These complexes all exhibit pentadentate $[N_3S_2]$ binding of the ligand to the metal centers. Like $[\mathbf{1}\text{-Zn}]^{2-}$, complexes $[\mathbf{1}\text{-Cd}]^{2-}$ and $[\mathbf{1}\text{-Hg}]^{2-}$ are C_2-symmetric in the solid state. These Zn, Cd, and Hg structures are best described as pseudo-square pyramidal (τ_5 closer to 0 than to 1).[10,11]

Table 1 compares the structural parameters of $[\mathbf{1}\text{-M}]^{2-}$ (M = Zn, Cd, and Hg). While the metal–pyridine bond distances (M–N2) increase in the expected order based on the ionic radius of the divalent cations, with Zn < Cd < Hg, the metal–thiolate (M–S) distances increase in the order of Zn < Hg ~ Cd. The slightly shorter metal–thiolate distances of $[\mathbf{1}\text{-Hg}]^{2-}$ compared to $[\mathbf{1}\text{-Cd}]^{2-}$ are consistent with previous comparisons of other mercury thiolate complexes with their cadmium thiolate congeners. These shorter Hg–X bonds compared to Cd–X bonds were previously proposed by Parkin and others to arise due to mercury's smaller covalent radius, as well as the influence of relativistic effects.[12] The larger metal cations also exhibited greater differences between the two metal–sulfur distances of each complex.

Comparison of metal thiolate nucleophilicity

The ^{1}H NMR spectra of DMSO-d_6 solutions of the products formed upon treatment of CH_3CN solutions of $[Et_4N]_2$[**1**-M] with MeI (1 equiv.) show singlet resonances corresponding to the methyl thioether moieties at δ 2.26 (M = Zn), 2.36 (M = Cd), and 2.41 (M = Hg) ppm, consistent with methylation of a single thiolate arm for each complex. We have previously reported that the addition of alkyl halides to $[\mathbf{1}\text{-Zn}]^{2-}$ results in thiolate alkylation to form helical bimetallic zinc complexes with pendant thioether moieties (Scheme 2, $[\mathbf{3}^{\mathbf{R}}\text{-Zn}]^{2-}$, R = Me, Et, Bn).[4,13] However, the aromatic regions of the ^{1}H NMR spectra of the methylated products for M = Cd^{2+} and Hg^{2+} differ from that of $[\mathbf{3}^{\mathbf{Me}}\text{-Zn}]^{2-}$, suggesting that thiolate methylation of these complexes exhibit different structures (Fig. S6 and S9).

The ^{113}Cd NMR spectrum of a DMSO-d_6 solution of the methylated cadmium congener shows a single resonance at −275.7 ppm, referenced against $Cd(ClO_4)_2$ (δ −640.27 ppm), indicating a single Cd chemical environment. This assignment is inconsistent with a bimetallic helical structure like that of $[\mathbf{3}^{\mathbf{Me}}\text{-Zn}]^{2-}$, in which the two metal centers have different coordination environments. Diffusion ordered NMR spectroscopy (DOSY) measured a diffusion coefficient of 1.62 × 10^{-10} m^2 s^{-1} for $[\mathbf{3}^{\mathbf{Me}}\text{-Zn}]^{2-}$, while that of the methylation product of $[\mathbf{1}\text{-Cd}]^{2-}$ is 1.84 × 10^{-10} m^2 s^{-1}. Based on these data and other DOSY NMR benchmarks of different metal complexes supported by this chelating ligand framework (Table S1), we assign the Cd and Hg methylation products to have monometallic structures (Fig. 2, $[\mathbf{4}^{\mathbf{Me}}\text{-M(solv)}]^{-}$, M = Cd, Hg, solv = CH_3CN or DMSO), in which the metal coordination

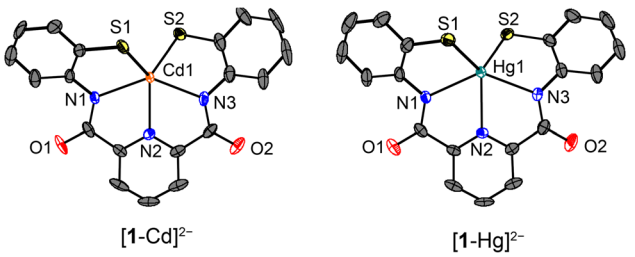

Fig. 1 Solid-state structures of $[Et_4N]_2$[**1**-M] (M = Cd, Hg) as 50% probability ellipsoids. Hydrogen atoms and tetraethylammonium cations omitted for clarity.

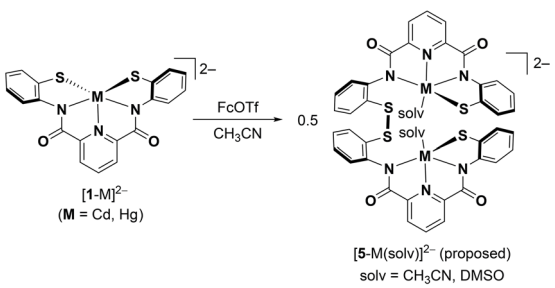

Scheme 2 Proposed disulfide product upon oxidation of $[\mathbf{1}\text{-M}]^{2-}$ (M = Cd, Hg).

Table 1 Selected structural parameters of metal(II) dithiolate complex ($[\mathbf{1}\text{-M}]^{2-}$, M = Zn, Cd, Hg)

	Bond length (Å)			Angle (°)		
M	M–S1	M–S2	M–N2	S1–M–S2	N1–M–N3	τ_5
Zn	2.3532(8)	2.3768(8)	2.118(2)	102.64(3)	147.67(10)	0.30(20)
Cd	2.5058(16)	2.5392(15)	2.308(4)	108.05(5)	137.69(15)	0.09(32)
Hg	2.4890(9)	2.5172(9)	2.420(3)	113.16(3)	133.22(9)	0.03(19)

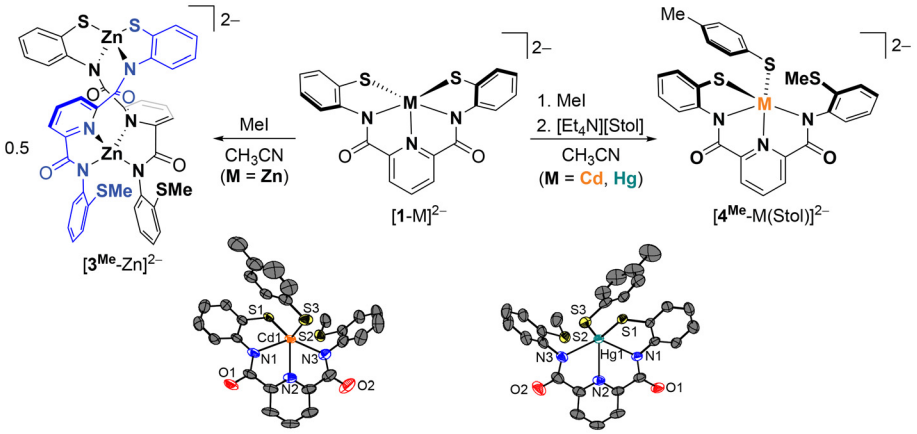

Fig. 2 Methylation of $[\mathbf{1}\text{-M}]^{2-}$ forms divergent metal-dependent structures. Solid-state structures of $[\mathbf{4^{Me}}\text{-Cd(Stol)}]^{2-}$ and $[\mathbf{4^{Me}}\text{-Hg(Stol)}]^{2-}$ are included as 50% probability ellipsoids. Countercations, hydrogen atoms, and solvent molecules not shown for clarity.

sphere is completed by coordinated solvent molecules. This difference reflects the larger ionic radii of these metals compared to Zn^{2+}, which more readily accommodates four-coordinate geometries.[14]

Although we have so far been unable to grow X-ray quality single crystals of $[\mathbf{4^{Me}}\text{-M(solv)}]^-$, addition of tetraethylammonium 4-methylbenzenethiolate ([Et$_4$N][Stol]) to $[\mathbf{4^{Me}}\text{-Cd(solv)}]^-$ or $[\mathbf{4^{Me}}\text{-Hg(solv)}]^-$ enabled the growth of single crystals of $[Et_4N]_2[\mathbf{4^{Me}}\text{-Cd(Stol)}]$ and $[Et_4N]_2[\mathbf{4^{Me}}\text{-Hg(Stol)}]$ (Fig. 2). Both complexes are monometallic with $[N_3S_2]$ coordination in which the methyl thioether moiety is not coordinated to the metal but displaced by the $^-$Stol anion. Addition of [Et$_4$N][Stol] to a DMSO-d_6 solution of $[Et_4N]_2[\mathbf{3^{Me}}\text{-Zn}]$ also forms a new species by ^{1}H NMR spectroscopy, indicating that the helical bimetallic structure of this complex can be disrupted by exogenous thiolate coordination.

To compare the influence of the different metal centers on the relative nucleophilicities of the thiolate moieties, competition experiments were performed by treatment of binary mixtures of different metal dithiolate complexes $[\mathbf{1}\text{-M}]^{2-}$ with MeI. As a representative dataset, Fig. 3 compares the ^{1}H NMR spectra of a 1 : 1 mixture of $[Et_4N]_2[\mathbf{1}\text{-Zn}]$ and $[Et_4N]_2[\mathbf{1}\text{-Cd}]$ in DMSO-d_6 with that of the same mixture measured 1 min after addition of MeI. The spectrum measured after addition of MeI shows a mixture of $[\mathbf{1}\text{-Zn}]^{2-}$, $[\mathbf{1}\text{-Cd}]^{2-}$, $[\mathbf{3^{Me}}\text{-Zn}]^{2-}$, and $[\mathbf{4^{Me}}\text{-Cd(solv)}]^-$. Integration of the spectrum showed that *ca.* 44% of $[\mathbf{1}\text{-Zn}]^{2-}$ was methylated compared to 15% of $[\mathbf{1}\text{-Cd}]^{2-}$. These results qualitatively suggest that the zinc thiolate moiety is more nucleophilic than the cadmium thiolate moiety.

We were unable to calculate the methylation reaction rate constants due to competitive metal cation exchange during the methylation reaction. For example, ^{1}H NMR spectroscopy of a DMSO-d_6 mixture of $[Et_4N]_2[\mathbf{1}\text{-Zn}]$ and $[Et_4N][\mathbf{4^{Me}}\text{-Cd(solv)}]$ showed the formation of $[\mathbf{3^{Me}}\text{-Zn}]^{2-}$ and $[\mathbf{1}\text{-Cd}]^{2-}$ over 1 h at room temperature (eqn (1), Fig. S28).

$$[\mathbf{1}\text{-Zn}]^{2-} + [\mathbf{4^{Me}}\text{-Cd(solv)}]^- \rightleftharpoons 0.5[\mathbf{3^{Me}}\text{-Zn}]^{2-} + [\mathbf{1}\text{-Cd}]^{2-} \quad (1)$$

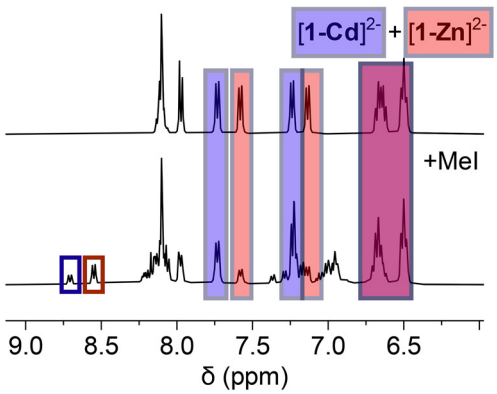

Fig. 3 ^{1}H NMR spectra of a 1 : 1 mixture of $[Et_4N]_2[\mathbf{1}\text{-Zn}]$ and $[Et_4N]_2[\mathbf{1}\text{-Cd}]$ in DMSO-d_6 before (top) and after (bottom) addition of MeI (1 equiv.), showing thiolate methylation. Shaded blue and red boxes correspond to resonances of $[\mathbf{1}\text{-Cd}]^{2-}$ and $[\mathbf{1}\text{-Zn}]^{2-}$, respectively, while resonances corresponding to $[\mathbf{4^{Me}}\text{-Cd(solv)}]^-$ and $[\mathbf{3^{Me}}\text{-Zn}]^{2-}$ are indicated with unshaded blue and red boxes, respectively.

Similar cation exchange reactions were observed between $[\mathbf{1}\text{-Zn}]^{2-}$ and $[\mathbf{4^{Me}}\text{-Hg(solv)}]^-$, and between $[\mathbf{1}\text{-Cd}]^{2-}$ and $[\mathbf{4^{Me}}\text{-Hg(solv)}]^-$ (Fig. S29 and S30).

Based on these results, the species observed in the spectra shown in Fig. 3 are likely formed from both thiolate alkylation and metal cation exchange. As metal cation exchange is apparently slower, on the order of tens of minutes, we approximated the spectrum taken immediately upon addition (<1 min) as arising only from thiolate alkylation. Table 2 shows the relative ratios for different mixtures. Based on these data, the thiolate nucleophilicities (k_M) of $[\mathbf{1}\text{-M}]^{2-}$ qualitatively decrease in the order $[\mathbf{1}\text{-Zn}]^{2-} > [\mathbf{1}\text{-Cd}]^{2-} > [\mathbf{1}\text{-Hg}]^{2-}$.

Although qualitative, the above results are consistent with previously reported experimental and theoretical measurements of metal thiolate nucleophilicity.[15,16] The greater nucleophilicity of $[\mathbf{1}\text{-Zn}]^{2-}$ compared to the cadmium and mercury congeners is consistent with the more ionic nature of

Table 2 Relative ratios of thiolate methylation estimated from ^{1}H NMR spectroscopy 1 min after addition of MeI

M^1	M^2	k_{M^1}/k_{M^2} [a]
Zn	Cd	2.6 ± 0.10
Zn	Hg	—[b]
Cd	Hg	1.41 ± 0.06

[a] Errors reported are standard deviations of triplicate measurements. [b] No [$\mathbf{4}^{\mathbf{Me}}$-Hg(solv)]$^-$ was observed in these reaction mixtures.

Table 3 Thiolate oxidation onset potentials (V *vs.* Fc^+/Fc) for $[\mathbf{1}\text{-M}]^{2-}$ complexes

M	E_{onset} [a] (V *vs.* Fc^+/Fc)
Zn	−0.59
Cd	−0.29
Hg	−0.25

[a] CVs measured at a scan rate of 100 mV s^{-1} of solutions in 0.1 M $TBAPF_6$ in CH_3CN using a glassy carbon working electrode, Pt wire counter electrode, and $AgNO_3$/Ag non-aqueous reference electrode.

the Zn–S bond compared to the Cd–S and Hg–S bonds, which are more covalent.[15]

Comparison of thiolate oxidation

We have previously reported that addition of chemical oxidants like ferrocenium trifluoromethanesulfonate (FcOTf) or I_2 to $[\mathbf{1}\text{-Zn}]^{2-}$ oxidized the thiolate moieties to form a disulfide-bridged bimetallic complex with a helical structure and two four-coordinate Zn^{2+} centers with two different coordination environments.[4] Treatment of CH_3CN solutions of $[\mathbf{1}\text{-M}]^{2-}$ (M = Cd, Hg) with FcOTf (1 equiv.) formed new yellow-brown products proposed to be disulfide-bridged complexes (Scheme 2, $[\mathbf{5}\text{-M(solv)}]^{2-}$). The ^{1}H NMR spectra of these species differ significantly from that of the oxidation product of $[\mathbf{1}\text{-Zn}]^{2-}$, possibly suggesting a different solution-state structure. The ^{113}Cd NMR spectrum of $[\mathbf{5}\text{-Cd}]^{2-}$ shows only a single resonance at δ −251.3 ppm, again inconsistent with the two different metal environments of the zinc disulfide structure. For these reasons, we assign $[\mathbf{5}\text{-Cd(solv)}]^{2-}$ and $[\mathbf{5}\text{-Hg(solv)}]^{2-}$ to the structure shown in Scheme 2, although we have not been able to able to structurally characterize these products by XRD. Negative ion mode electrospray ionization mass spectrometry (ESI-MS) of $[\mathbf{5}\text{-M(solv)}]^{2-}$ (M = Cd, Hg) shows molecular ion peaks at 1002.1409 *m*/z ($[\mathbf{5}\text{-Cd}]$ + Na)$^-$, and 1157.0058 *m*/*z* ($[\mathbf{5}\text{-Hg}]$ + H)$^-$, respectively, consistent with the expected values for the corresponding $[\mathbf{5}\text{-M}]^{2-}$ ions without coordinated solvent.

The above results point to metal-dependent structural differences upon thiolate oxidation. The cyclic voltammograms (CVs) of CH_3CN solutions of $[Et_4N]_2[\mathbf{1}\text{-M}]$ (M = Zn, Cd, Hg) with $TBAPF_6$ electrolyte (TBA = tetrabutylammonium, 0.1 M) were measured (Fig. S38). Each voltammogram shows two broad, irreversible oxidation waves between −0.6 and 0.1 V *vs.* Fc^+/Fc corresponding to oxidation of the thiolate moieties. The return reduction waves observed in the voltammograms are assigned to reduction of disulfide moieties formed after thiolate oxidation. Table 3 compares the onset potentials of the first thiolate oxidation waves for each complex, which shift to more positive potentials in the order $[\mathbf{1}\text{-Zn}]^{2-} < [\mathbf{1}\text{-Hg}]^{2-} \sim [\mathbf{1}\text{-Cd}]^{2-}$. The more positive oxidation potentials of the cadmium and mercury congeners may correspond to the greater covalency of the M–S bonds in these compounds. These electrochemically measured differences are consistent with the reactivity of these complexes. A DMSO-d_6 mixture of $[\mathbf{5}\text{-Cd(solv)}]^{2-}$ and $[\mathbf{1}\text{-Zn}]^{2-}$ showed reduction of the former and oxidation of the latter by ^{1}H NMR spectroscopy (Fig. S39).

Reactions of metal thiolates with sulfur

Complex $[\mathbf{1}\text{-Zn}]^{2-}$ was previously reported to selectively insert three "S^0" atom equivalents to form the zinc tetrasulfanide complex $[\mathbf{2}\text{-Zn}]^{2-}$ upon treatment with S_8 (Scheme 1a).[4,17] Although sulfur exchange in this complex is dynamic in solution, as demonstrated from isotopic labelling with $^{34}S_8$,[17] this reaction proceeds cleanly in both acetonitrile and DMSO, even with excess S_8, with no observed formation of disulfanide, trisulfanide, or higher order polysulfanide products.[4] Further, sulfur insertion is only observed at one of the two thiolate donors. In contrast, when DMSO-d_6 solutions of $[\mathbf{1}\text{-Cd}]^{2-}$ or $[\mathbf{1}\text{-Hg}]^{2-}$ were treated with 3 S atom equivalents of S_8 (*i.e.*, 3/8 equiv. S_8), ^{1}H NMR spectroscopy showed the formation of a mixture of two major new products, as well as remaining $[\mathbf{1}\text{-M}]^{2-}$. Complete consumption of $[\mathbf{1}\text{-Cd}]^{2-}$ was only observed upon further S_8 addition (>5 S atom equivalents). The formation of these products is reversible; addition of PPh_3 to these reaction mixtures abstracts S^0 to form $SPPh_3$ in an equimolar amount as the S_8 added, per S atom, and regenerate $[\mathbf{1}\text{-M}]^{2-}$ (M = Cd, Hg).

Fig. 4 compares the ^{1}H NMR spectra of a DMSO-d_6 solution of $[Et_4N]_2[\mathbf{1}\text{-Cd}]$ with added S_8 (3/8 and 5/8 equiv.). One of these products is a C_1-symmetric product with a downfield doublet resonance at δ 8.47 ppm, similar to that of $[\mathbf{2}\text{-Zn}]^{2-}$

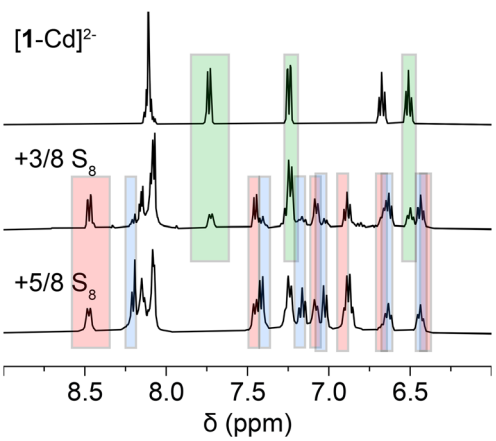

Fig. 4 ^{1}H NMR spectra of a DMSO-d_6 solution of $[Et_4N]_2[\mathbf{1}\text{-Cd}]$ before (top) and after addition of S_8 (3/8 equiv., middle and 5/8 equiv., bottom). Green boxes indicate $[\mathbf{1}\text{-Cd}]^{2-}$, red boxes indicate the C_1-symmetric product $[\mathbf{2}\text{-Cd}]^{2-}$, and blue boxes indicate $[\mathbf{6}\text{-Cd}]^{2-}$.

(Fig. S32) and is assigned as the cadmium tetrasulfanide complex [**2**-Cd]$^{2-}$ (Scheme 3). The downfield shift of the resonance is attributed to structural distortions resulting in closer interactions between the oxygen atom of the amide and an arene ring in the ligand framework. A second C_2- or C_s-symmetric species ([**6**-Cd]$^{2-}$) is also present in the mixture, whose concentration increases with further addition of S_8. Due to the symmetry of this complex and its formation from [**2**-Cd]$^{2-}$, we currently assign this species as the bis(tetrasulfanide) complex shown in Scheme 3 but cannot rule out sulfur rearrangement within this complex. These mixtures are assigned as equilibrium mixtures rather than slow, incomplete reactions, as the NMR spectra measured initially upon S_8 addition do not change over 12 h.

As these species exist in dynamic exchange with [**1**-Cd]$^{2-}$ (at lower S_8 concentrations) and with excess S_8, we have so far been unable to cleanly isolate these complexes or to characterize them by XRD. However, ESI-MS of these mixtures are consistent with this assignment (Fig. S44–S47). For example, ESI-MS of a mixture of [**1**-Cd]$^{2-}$ and 5/8 S_8 shows molecular ion peaks at 587.8581 *m/z* corresponding to [**2**-Cd]$^{2-}$ + H (with three added S atoms) and at 683.7771 *m/z*, corresponding to [**6**-M]$^{2-}$ + H, although additional ion peaks corresponding to sulfur–sulfur fragmentation are also observed. These signals shift as expected when isotopically enriched $^{34}S_8$ is used. DOSY NMR of this mixture is also consistent with the assigned monometallic structures, with both species exhibiting a diffusion coefficient of 1.73×10^{-10} m^2 s^{-1}.

Using these proposed stoichiometries, the equilibrium constants for the formation of [**2**-M]$^{2-}$ (K_1) and [**6**-M]$^{2-}$ (K_2, M = Cd, Hg) were calculated by integration of the ^{1}H NMR spectra of mixtures containing [**1**-M]$^{2-}$, [**2**-M]$^{2-}$, and [**6**-M]$^{2-}$, where $K_1^{M} = \dfrac{[\mathbf{2}\text{-M}]}{[\mathbf{1}\text{-M}][S_8]^{\frac{3}{8}}}$ and $K_2^{M} = \dfrac{[\mathbf{6}\text{-M}]}{[\mathbf{2}\text{-M}][S_8]^{\frac{3}{8}}}$. For the cadmium congener, these values were found to be $K_1^{Cd} = 14 \pm 4$ M$^{-\frac{3}{8}}$ and $K_2^{Cd} = 1.1 \pm 0.1$ M$^{-\frac{3}{8}}$. For the mercury complex, these values were $K_1^{Hg} = 7 \pm 2$ M$^{-\frac{3}{8}}$ and $K_2^{Hg} = 5 \pm 1$ M$^{-\frac{3}{8}}$. These equilibrium constants differ from those of sulfur insertion into the Zn–S bond of [**1**-Zn]$^{2-}$. For the zinc congener, the first sulfur insertion reaction exhibits a high equilibrium constant and is complete even upon addition of 3/8 equiv. of S_8 ($K_1^{Zn} \gg K_1^{Cd} > K_1^{Hg}$). The second sulfur insertion process is not observed for the zinc complex ($K_2^{Zn} \ll K_2^{Cd} < K_2^{Hg}$).

If the polysulfanide mixtures of [**2**-Cd]$^{2-}$ and [**6**-Cd]$^{2-}$or of [**2**-Hg]$^{2-}$ and [**6**-Cd]$^{2-}$ in DMSO are heated in the presence of moisture, protonolysis and demetallation occur alongside ligand oxidation, forming a previously reported trisulfide-bridged bis(carboxamide)pyridine framework.[17] When heated under anhydrous conditions, [Et$_4$N]$_2$[**2**-Cd] converted to a new D_2-symmetric product (^{1}H NMR spectroscopy, [**7**]$^{2-}$). The XRD structure of [Et$_4$N]$_2$[**7**] shows the anion to contain a six-coordinate cadmium complex in which two pyridine carboxamide ligands are bridged by trisulfide moieties (Fig. 5). A similar zinc congener was previously reported upon the treatment of [Et$_4$N]$_2$[**2**-Zn] with the electrophilic alkyne dimethyl acetylenedicarboxylate.[17] As the formation of this pseudo-octahedral complex corresponds to a formal oxidation of the bis(carboxamide)pyridine dithiolate ligand and reduction of sulfur, the byproduct is presumed to be precipitated CdS. Similarly, when a solution of [Et$_4$N]$_2$[**6**-Hg] was heated under anhydrous conditions, HgS was observed as a byproduct (power X-ray diffraction, Fig. S41), along with a demetallated trisulfide-bridged bis(carboxamide)pyridine compound.[17]

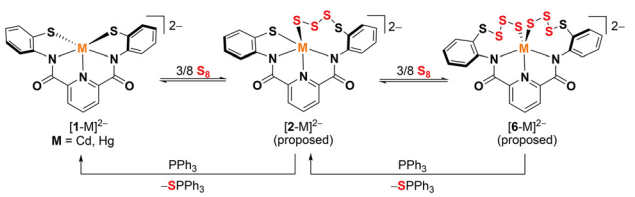

Scheme 3 Sulfur insertion into the M–S bonds of [**1**-Cd]$^{2-}$ and [**1**-Hg]$^{2-}$.

Computational studies

The experimental data were supported by density functional theory (DFT) calculations using the ORCA 6.1.0 software package.[18–22] The conformational space was explored using the Conformer-Rotamer Ensemble Sampling Tool (CREST 3.0.2) at the GFN2-xTB level of theory using the GBSA solvation model for dimethyl sulfoxide.[23–25] All found conformers were subsequently reoptimized at the DFT/ωB97X-D4/def2-TZVPPD level of theory using the SMD solvation model for dimethyl sulfoxide.[26–28] Conformers within an energetic window of 12.6 kJ mol^{-1} were further refined by single-point calculations at the DFT/ωB97X-D4/def2-QZVPPD level of theory using the SMD solvation model for dimethyl sulfoxide. The functional ωB97X-D4 with a basis set of quadruple-zeta (QZ) was chosen since it is recommended for conformer and reaction energy calculations.[29] The basis sets with diffuse functions were chosen to accurately describe the anions.[29] Harmonic vibrational frequencies were calculated at both the TZ and QZ

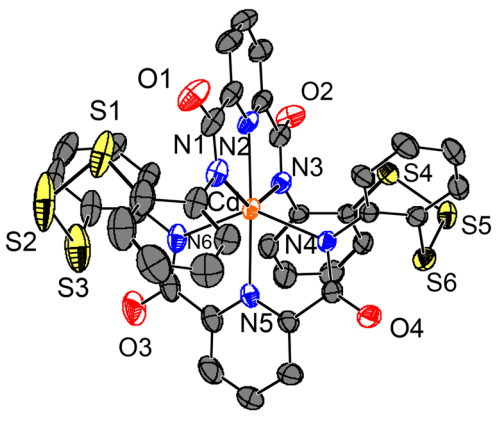

Fig. 5 Solid-state structure of [Et$_4$N]$_2$[**7**] as 50% probability ellipsoids. Tetraethylammonium countercations, hydrogen atoms, and a water molecule not shown for clarity.

level, while the QZ level was used to compute thermodynamic properties. When multiple relevant conformers were found, they were included in a Boltzmann-weighted structure ensemble (SE) as suggested by Grimme *et al.* to ensure that conformational populations are properly reflected in the calculated thermodynamics.[29,30] Further computational details are provided in the SI.

Since no experimental crystal structures could be obtained for the complexes $[\mathbf{2}\text{-Cd}]^{2-}$ and $[\mathbf{6}\text{-Cd}]^{2-}$ (Scheme 3), the change in Gibbs free energy (ΔG) for the two proposed sulfur insertion steps was calculated (eqn (2)).

$$\Delta G = G_{\mathrm{SE}}^{\mathrm{X+3S}} - \left(G_{\mathrm{SE}}^{\mathrm{X}} + \frac{3}{8}G^{\mathrm{S_8}}\right) \tag{2}$$

For the formation of $[\mathbf{2}\text{-Cd}]^{2-}$ from $[\mathbf{1}\text{-Cd}]^{2-}$, the Gibbs free energy was found to be −20.7 kJ mol^{-1}. The energy of the second insertion step to form $[\mathbf{6}\text{-Cd}]^{2-}$ from $[\mathbf{2}\text{-Cd}]^{2-}$ was found to be −25.7 kJ mol^{-1}. These calculations show that both sulfur insertion steps are favorable, consistent with the experimental results. However, these calculated energies are higher than expected, based on the observed equilibrium constants K_1^{Cd} and K_2^{Cd}.

We also considered a second possible isomer of the C_1-symmetric 3 S-atom insertion product, in which two sulfur atoms insert at one thiolate arm, and one sulfur atom inserts at the second ($[\mathbf{2}'\text{-Cd}]^{2-}$, Scheme 4). Based solely on the calculated Gibbs free energies, the formation of both $[\mathbf{2}\text{-Cd}]^{2-}$ and $[\mathbf{2}'\text{-Cd}]^{2-}$ seems thermodynamically feasible, with $[\mathbf{2}\text{-Cd}]^{2-}$ as the more stable isomer by −6.4 kJ mol^{-1}. This assessment does not take any reaction barriers into account.

For further insights, the frontier molecular orbitals were considered as shown in Fig. 6. The lowest unoccupied molecular orbital (LUMO) shows strongly ligand-centered character on the pyridine backbone of the ligand for all cadmium complexes considered ($[\mathbf{1}\text{-Cd}]^{2-}$, $[\mathbf{2}\text{-Cd}]^{2-}$, $[\mathbf{2}'\text{-Cd}]^{2-}$ and $[\mathbf{6}\text{-Cd}]^{2-}$). However, the highest occupied molecular orbitals (HOMO) vary after sulfur insertion. The HOMO of the dithiolate complex $[\mathbf{1}\text{-Cd}]^{2-}$ is localized on the sulfur atoms of the thiolate donors, consistent with the observed nucleophilic reactivity of this complex. Similarly, the HOMO of $[\mathbf{2}\text{-Cd}]^{2-}$ is centered on the sulfur of the remaining thiolate donor, with little contribution from the sulfur atoms of the tetrasulfanide moiety. In contrast, the HOMO of complex $[\mathbf{2}'\text{-Cd}]^{2-}$ shows contribution from both the trisulfanide and disulfanide "arms" of the complex.

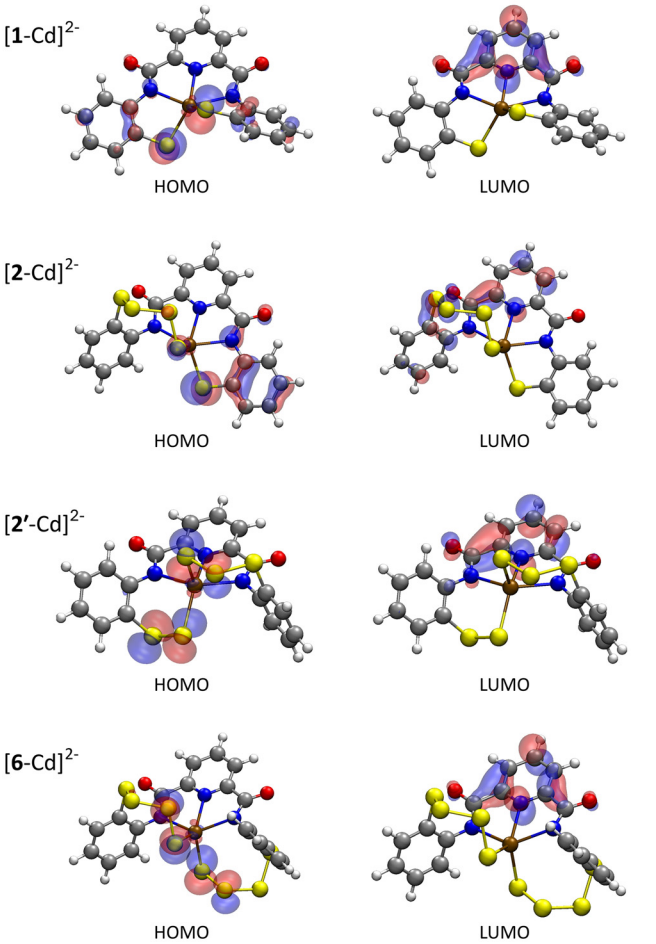

Fig. 6 Frontier molecular orbitals for the most stable conformers of Cd complexes at ωB97X-D4/def2-QZVPPD/SMD(dmso)//ωB97X-D4/def2-TZVPPD/SMD(dmso) level of theory (isovalue = 0.05).

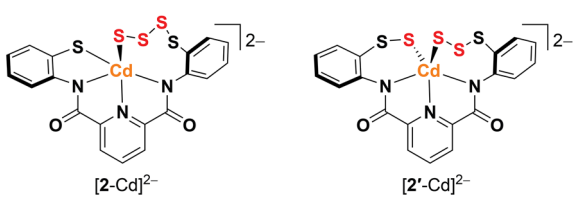

Scheme 4 Possible products of sulfur insertion into the Cd–S(thiolate) bonds of $[\mathbf{1}\text{-Cd}]^{2-}$ at ωB97X-D4/def2-QZVPPD/SMD(dmso)//ωB97X-D4/def2-TZVPPD/SMD(dmso) level of theory.

As a qualitative analysis of these frontier orbital pictures, the HOMO of $[\mathbf{1}\text{-Cd}]^{2-}$ appears to be consistent with the formation of either $[\mathbf{2}\text{-Cd}]^{2-}$ or $[\mathbf{2}'\text{-Cd}]^{2-}$ upon nucleophilic attack of the thiolate groups of $[\mathbf{1}\text{-Cd}]^{2-}$ on an S_8 molecule. However, as the second sulfur insertion step forms a C_2- or C_s-symmetric complex such as $[\mathbf{6}\text{-Cd}]^{2-}$, we favor the intermediacy of structure $[\mathbf{2}\text{-Cd}]^{2-}$ as the product of the first sulfur insertion step. Based on the HOMO of $[\mathbf{2}'\text{-Cd}]^{2-}$, there appears to be little electronic distinction between the two "arms" of the complex, possibly resulting in a greater mixture of products upon a second sulfur insertion step. This rough analysis does not account for thermodynamically-driven exchange, however.

Discussion

The results above demonstrate that different divalent metal complexes of the same chelating dithiolate ligand result in different reactivity toward sulfur. Substitution of Zn^{2+} for

larger divalent metal cations (Cd^{2+} and Hg^{2+}) qualitatively appears to attenuate sulfur insertion into the metal–S(thiolate) bond. Whereas $[\mathbf{1}\text{-Zn}]^{2-}$ is completely converted upon addition of 3/8 equiv. S_8, $[\mathbf{1}\text{-Cd}]^{2-}$ and $[\mathbf{1}\text{-Hg}]^{2-}$ both show smaller equilibrium constants for the first sulfur insertion reaction. Additionally, while only one thiolate moiety of the zinc congener undergoes sulfur insertion/catenation, both $[\mathbf{1}\text{-Cd}]^{2-}$ and $[\mathbf{1}\text{-Hg}]^{2-}$ can insert sulfur at both thiolate arms.

As discussed above, we presume that the sulfur insertion reaction proceeds by nucleophilic attack of the thiolate moiety on S_8, followed by S_8 ring-opening. The thiolate moieties of $[\mathbf{1}\text{-Zn}]^{2-}$ are more nucleophilic than those of $[\mathbf{1}\text{-Cd}]^{2-}$ and $[\mathbf{1}\text{-Hg}]^{2-}$, as might be predicted from metal–sulfur covalency. However, as sulfur insertion into the metal thiolate complexes has been demonstrated to undergo fast exchange, the resulting tetrasulfanide complexes are thermodynamically stabilized rather than kinetically trapped.[17] For these reasons, the nucleophilicity of the thiolate moiety is unlikely to be the major influence over metal-dependent sulfur reactivity. Similarly, when considering the thiolate oxidation potential as a proxy for electron availability, the minor shifts in potentials upon metal substitution are not consistent with the observed differences in sulfur insertion reactivity.

We hypothesize that the different geometries around the metal centers are the major factor influencing sulfur insertion reactivity, as these likely also affect the resulting stability of the polysulfanide products as well as the strain of the initial thiolate chelate itself. We have previously demonstrated that for tris(pyrazolyl)borate-supported zinc thiolate complexes, only the strained chelating 2-thiopyridine derivative was observed to insert sulfur upon treatment with S_8.[5] Although $[\mathbf{1}\text{-Zn}]^{2-}$, $[\mathbf{1}\text{-Cd}]^{2-}$, and $[\mathbf{1}\text{-Hg}]^{2-}$ all show similar C_2-symmetric geometries, the ∠S–M–S angles increase from Zn to Cd to Hg, perhaps indicating a decrease in thiolate–thiolate repulsion. When $[\mathbf{1}\text{-Zn}]^{2-}$ reacts with S_8 to form $[\mathbf{2}\text{-Zn}]^{2-}$, the ∠S–Zn–S angle increases from 102.64(3)° to 106.66°, showing a decrease in this sulfur–sulfur interaction. Sulfur insertion is less favored for $[\mathbf{1}\text{-Cd}]^{2-}$ and $[\mathbf{1}\text{-Hg}]^{2-}$ due to less of this repulsion within the dithiolate complexes. Similarly, for these reasons, sulfur insertion into the second thiolate arm is close in energy to that of sulfur insertion into the first thiolate arm, therefore forming two types of polysulfanide products.

Although this present study serves primarily as a simple description of coordination chemistry differences, these results may have broader implications for biological metal–thiolate motifs. For example, metallothioneins bind zinc, cadmium, and mercury, but have also been proposed to undergo persulfidation.[31] While the regulatory role of such structures have yet to be determined, our results may indicate that metal substitution would affect incorporation of sulfane sulfur.

Conclusions

This study compared sulfur insertion into the metal–thiolate bonds of dianionic dithiolate complexes of different divalent metal ions. Larger cations showed less favorable sulfur insertion equilibria, as well as decreased selectivity. Although this behavior also correlates somewhat with increasing metal–sulfur covalency for larger cations, we primarily attribute these reactivity differences to changes in complex geometry induced by the different cation sizes and resulting strain within the complex itself. These results suggest that intra-ligand effects are critical for controlling the reactivity of metal thiolate moieties.

Experimental section

General considerations

Unless otherwise indicated, all reactions were conducted using oven-dried glassware in an MBraun glovebox under a purified nitrogen atmosphere or using a Schlenk line. Anhydrous solvents, including diethyl ether (Et_2O), THF, toluene, hexanes, and CH_3CN, were dried by the Grubbs method using a J.C. Meyer solvent purification system.[32] Deuterated solvents were purchased from Cambridge Isotope Laboratories. DMSO-d_6 was dried over CaH_2, distilled under vacuum, and stored under nitrogen over 4 Å activated molecular sieves. CD_3CN was dried over CaH_2 and vacuum transferred before use. Celite was dried under vacuum at 300 °C for 3 d.

^1H and ^{13}C NMR spectra were recorded on Bruker 400 MHz, Bruker 500 MHz, or Varian 600 MHz instruments, with chemical shifts referenced to the residual solvent peaks (^1H, δ 2.50 ppm and ^{13}C, δ 39.5 ppm for DMSO-d_6; ^1H, δ 7.26 ppm and ^{13}C, δ 77.16 ppm for $CDCl_3$; ^1H, δ 1.94 ppm for CD_3CN). ^{113}Cd NMR spectra were externally referenced to $Cd(ClO_4)_2$ in H_2O (δ −640.27 ppm) and ^{31}P NMR spectra were referenced to phosphoric acid (H_3PO_4, δ 0 ppm). Elemental analyses were performed by Midwest Microlabs, LLC, in Indianapolis, IN.

Caution! Cadmium and mercury compounds are highly toxic and should be handled with appropriate care.

Synthesis of $[Et_4N]_2[\mathbf{1}\text{-M}]$

In a representative procedure for M = Cd, in the glovebox, a scintillation vial equipped with a stir bar was charged with H_4L (0.250 g, 0.66 mmol, 1 equiv.) and CH_3CN (4 mL). The mixture was frozen in a cold well cooled with liquid nitrogen. Upon thawing, NaHMDS (0.481 g, 2.64 mmol, 4 equiv.) dissolved in 2 mL of THF was added in parts. The mixture was allowed to stir for 10 min, during which the solution turned yellow. A solution of Et_4NCl (0.434 g, 2.62 mmol, 2 equiv.) and $CdCl_2$ (0.120 g, 0.66 mmol, 1 equiv.) in CH_3CN (6 mL) was added dropwise to the reaction mixture, and the mixture turned orange-yellow. The mixture was stirred for 1 h and allowed to warm up room temperature. After filtration through Celite, the solvent was reduced *in vacuo*. Bright orange crystals were grown by vapor diffusion of diethyl ether into the CH_3CN filtrate. The crystals were collected by filtration and washed with THF, hexanes, and diethyl ether, then dried under vacuum.

$[Et_4N]_2$[**1**-Cd]. Yield: 0.314 g (64%). ^{1}H NMR (400 MHz, DMSO-d_6) δ 8.17–8.05 (m, 3H), 7.74 (dd, J = 7.5, 2H), 7.24 (dd, J = 7.5, 2H), 6.67 (td, J = 7.5, 2H), 6.51 (td, J = 7.5, 2H), 3.13 (q, J = 7.2, 16H), 1.19–1.01 (t, J = 7.2, 24H). ^{13}C NMR (101 MHz, DMSO-d_6): δ 161.44, 152.10, 147.40, 143.60, 139.54, 131.64, 123.48, 121.06, 119.49, 119.42, 51.35, 7.02. ^{113}Cd NMR (89 MHz) δ −138.81. Anal. calcd for $C_{35}H_{51}N_5O_2S_2Cd$: C, 56.02; H, 6.85; N, 9.33. Found: C, 56.01; H, 6.86; N, 9.35.

$[Et_4N]_2$[**1**-Hg]. Yield: 0.490 g (56%). ^{1}H NMR (400 MHz, DMSO-d_6) δ 8.16 (dd, J = 8.2, 2H), 8.05 (dd, J = 8.2, 1H), 7.71 (dd, J = 7.8, 2H), 7.27 (dd, J = 7.8, 2H), 6.71 (, J = 7.4, 2H), 6.54 (t, J = 7.4, 2H), 3.13 (q, J = 7.2 Hz, 16H), 1.15 (t, J = 7.2 Hz, 24H). ^{13}C NMR (101 MHz, DMSO-d_6) δ 161.74, 152.09, 147.30, 141.84, 138.41, 130.91, 123.73, 121.29, 120.00, 119.12, 51.35, 7.02. Anal. calcd for $C_{35}H_{51}N_5O_2S_2Hg$: C, 50.13; H, 6.13; N, 8.35. Found: C, 50.12; H, 6.01; N, 8.43.

Synthesis of $[Et_4N][4^{Me}$-M(CH$_3$CN)] (M = Cd, Hg)

In a representative procedure, in the glovebox, a 50 mL Schlenk flask equipped with a stir bar was charged with $[Et_4N]_2$[**1**-M] and CH_3CN. The flask was removed from the glovebox and put under a N_2 atmosphere on the Schlenk line. MeI was added by syringe, and the reaction mixture stirred at room temperature for 30 min. The reaction mixture was concentrated to 2 mL *in vacuo*. The resulting yellow precipitate was filtered in the glovebox, washed with Et_2O, THF, and cold CH_3CN, then dried *in vacuo* to yield the product, which was used without further purification.

$[Et_4N][4^{Me}$-Cd(CH$_3$CN)]. $[Et_4N]_2$[**1**-Cd] (0.469 g, 0.63 mmol, 1 equiv.) and CH_3CN (20 mL) and MeI (38.9 μL, 0.63 mmol, 1 equiv.) was added by Hamilton syringe. Yield: 0.240 g (60%). ^{1}H NMR (400 MHz, DMSO-d_6) δ 8.72 (d, J = 7.7 Hz, 1H), 8.20 (t, J = 8.7 Hz, 1H), 8.15 (d, J = 7.4 Hz, 1H), 7.30 (d, J = 7.4 Hz, 1H), 7.24 (td, J = 8.0, 1H), 7.08 (t, J = 8.0 Hz, 1H), 6.96 (t, J = 8.0, 1H), 6.70 (t, J = 8.0 Hz, 1H), 6.50 (t, J = 7.4 Hz, 1H), 3.15 (q, J = 7.2 Hz, 8H), 2.37 (s, 3H), 1.21–1.02 (q, J = 7.2, 12H). ^{13}C NMR (101 MHz, DMSO-d_6) δ 161.38, 152.19, 149.87, 148.23, 145.93, 140.38, 139.29, 131.66, 131.32, 125.59, 125.41, 124.46, 122.24, 121.79, 121.62, 121.49, 120.88, 119.36, 51.41, 51.38, 51.35, 15.71, 7.05. ^{113}Cd NMR (89 MHz) δ −275.60.

$[Et_4N][4^{Me}$-Hg(CH$_3$CN)]. $[Et_4N]_2$[**1**-Hg] (0.724 g, 0.86 mmol, 1 equiv.) and CH_3CN (15 mL) and MeI (54 μL, 0.86 mmol, 1 equiv.) was added by Hamilton syringe. Yield: 0.384 g (53%). ^{1}H NMR (400 MHz, DMSO-d_6) δ 8.71 (d, J = 8.0 Hz, 1H), 8.28 (dd, J = 8.0 Hz, 1H), 8.21–8.11 (m, 2H), 7.36–7.23 (m, 3H), 7.20–7.01 (m, 2H), 6.80 (t, J = 7.6 Hz, 1H), 6.58 (t, J = 7.6 Hz, 1H), 3.17 (q, J = 7.2 Hz, 8H), 2.39 (s, 3H), 1.18–1.07 (t, J = 7.2 Hz, 12H). ^{13}C NMR (101 MHz, DMSO-d_6) δ 163.00, 161.88, 151.35, 147.33, 147.13, 144.53, 140.41, 132.39, 131.26, 129.44, 126.48, 125.65, 124.66, 123.43, 123.38, 122.71, 122.44, 121.53, 51.40, 51.37, 51.34, 14.84, 7.03.

Synthesis of $[Et_4N]_2[4^{Me}$-M(Stol)] (M = Cd, Hg)

In a representative procedure, in the glovebox, a 20 mL scintillation vial equipped with a stir bar was charged with $[Et_4N][4^{Me}$-M(CH$_3$CN)] and CH_3CN. $[Et_4N][Stol]$ was added dropwise as a solution in CH_3CN. After 10 min at room temperature, the reaction mixture was dried under vacuum. The resulting residue was washed with ether and THF, then recrystallized from CH_3CN/Et_2O.

$[Et_4N]_2[4^{Me}$-Cd(Stol)]. $[Et_4N][4^{Me}$-Cd(CH$_3$CN)] (0.210 g, 0.33 mmol, 1 equiv.) and CH_3CN (5 mL). $[Et_4N][Stol]$ (0.083 g, 0.33 mmol, 1 equiv.) was added as a solution in CH_3CN (2 mL). Yield: 0.234 g (81%). ^{1}H NMR (400 MHz, DMSO-d_6) δ 8.41 (d, J = 7.4 Hz, 1H), 8.09 (m, 3H), 7.27 (d, J = 8.3 Hz, 1H), 7.05 (d, J = 7.4 Hz, 1H), 6.96–6.82 (m, 2H), 6.68 (d, J = 8.3 Hz, 2H), 6.47 (t, J = 7.4 Hz, 1H), 6.33–6.19 (d, J = 8.3 Hz, 1H), 3.08 (q, J = 7.2 Hz, 16H), 2.24 (s, 3H), 1.96 (s, 3H), 1.04 (t, J = 7.2 Hz, 24H). ^{13}C NMR (101 MHz, DMSO-d_6) δ 161.24, 153.40, 147.15, 139.05, 132.16, 131.77, 127.34, 123.61, 122.10, 121.49, 121.06, 119.93, 118.99, 118.09, 51.43, 51.40, 51.37, 40.20, 39.99, 39.78, 39.57, 39.36, 39.15, 38.94, 25.15, 20.33, 7.06. ^{113}Cd NMR (89 MHz) δ −178.03. Anal. calcd for $C_{43}H_{61}N_5O_2S_3Cd$: C, 58.12; H, 6.92; N, 7.88. Found: C, 58.59; H, 6.95; N, 7.70.

$[Et_4N]_2[4^{Me}$-Hg(Stol)]. $[Et_4N][4^{Me}$-Hg(CH$_3$CN)] (0.105 g, 0.32 mmol, 1 equiv.) and CH_3CN (5 mL). $[Et_4N][Stol]$ (0.037 g, 0.32 mmol, 1 equiv.) was added as a solution in CH_3CN (2 mL). Yield: 0.107 g (77%). ^{1}H NMR (400 MHz, DMSO-d_6) δ 8.38 (d, J = 7.6 Hz, 1H), 8.25 (d, J = 7.6 Hz, 1H), 8.12 (d, J = 7.3 Hz, 1H), 7.95 (t, J = 7.3 Hz, 1H), 7.57 (d, J = 7.3 Hz, 1H), 7.32 (d, J = 7.3 Hz, 1H), 6.97 (d, J = 7.3 Hz, 1H), 6.9–6.74 (m, 5H), 6.72 (t, J = 6.5 Hz, 1H), 6.53 (t, J = 6.5 Hz, 1H), 6.44 (d, J = 8.1 Hz, 2H), 3.07 (q, J = 7.2 Hz, 16H), 2.24 (s, 3H), 2.02 (s, 3H), 1.04 (t, J = 7.2 Hz, 24H). ^{13}C NMR (101 MHz, DMSO-d_6) δ 162.73, 162.42, 154.29, 153.41, 150.51, 146.82, 137.49, 133.32, 131.22, 130.80, 128.94, 127.82, 124.52, 123.41, 123.02, 122.58, 122.34, 121.99, 121.15, 120.14, 118.78, 51.57, 51.54, 51.51, 20.44, 14.44, 7.19. Anal. calcd for $C_{43}H_{61}N_5O_2S_3Hg$: C, 53.65; H, 6.39; N, 5.82. Found: C, 53.91; H, 6.21; N, 5.41.

Conflicts of interest

There are no conflicts to declare.

Data availability

Additional data have been included as part of the supplementary information (SI). Supplementary information: NMR, UV–vis, mass spectrometry, and CV data. See DOI: https://doi.org/10.1039/d6dt00074f.

CCDC 2521016–2521020 ($[Et_4N]_2$[**1**-M], $[Et_4N]_2[4^{Me}$-M(Stol)] (M = Cd, Hg), and $[Et_4N]_2$[**7**]) contain the supplementary crystallographic data for this paper.[33a–e]

Acknowledgements

This work was supported by the NSF (CHE-2047045). Financial support from the German Academic Exchange Service (fellowship for C. H. through the ISAP program) is gratefully acknowledged. Diffraction instruments used in this project were sup-

ported by NSF MRI CHE-2214606. We thank Dr Evgenii Kovrigin for assistance with NMR spectroscopy and Nonka Sevova for assistance with mass spectrometry. This research was supported in part by the Notre Dame Center for Research Computing through its high-performance computing resources.

Notes and references

1 S. Jungen, E. Paenurk and P. Chen, *Inorg. Chem.*, 2020, **59**, 12322–12336.
2 K. Li, L. N. Zakharov and M. D. Pluth, *J. Am. Chem. Soc.*, 2023, **145**, 13435–13443.
3 W. T. M. Seo, M. N. Riffel, A. G. Oliver and E. Y. Tsui, *Chem. Sci.*, 2024, **15**, 7332–7341.
4 M. Ballesteros II and E. Y. Tsui, *Inorg. Chem.*, 2019, **58**, 10501–10507.
5 W. T. M. Seo, V. A. Tsang, M. Ballesteros II and E. Y. Tsui, *Chem. – Eur. J.*, 2024, **30**, e202401280.
6 M. Margoshes and B. L. Vallee, *J. Am. Chem. Soc.*, 1957, **79**, 4813–4814.
7 M. J. Stillman, *Coord. Chem. Rev.*, 1995, **144**, 461–511.
8 Y. He, M. Liu, N. Darabedian, Y. Liang, D. Wu, J. Xiang and F. Zhou, *Inorg. Chem.*, 2014, **53**, 2822–2830.
9 H. Shindo and T. L. Brown, *J. Am. Chem. Soc.*, 1965, **87**, 1904–1909.
10 A. W. Addison, T. N. Rao, J. Reedijk, J. van Rijn and G. C. Verschoor, *J. Chem. Soc., Dalton Trans.*, 1984, 1349–1356.
11 A. G. Blackman, E. B. Schenk, R. E. Jelley, E. H. Krenske and L. R. Gahan, *Dalton Trans.*, 2020, **49**, 14798–14806.
12 J. G. Melnick, K. Yurkerwich and G. Parkin, *J. Am. Chem. Soc.*, 2010, **132**, 647–655.
13 W. T. M. Seo, M. Ballesteros II and E. Y. Tsui, *J. Am. Chem. Soc.*, 2022, **144**, 20630–20640.
14 A. Krężel and W. Maret, *Arch. Biochem. Biophys.*, 2016, **611**, 3–19.
15 D. C. Fox, A. T. Fiedler, H. L. Halfen, T. C. Brunold and J. A. Halfen, *J. Am. Chem. Soc.*, 2004, **126**, 7627–7638.
16 M. Gennari, M. Retegan, S. DeBeer, J. Pécaut, F. Neese, M.-N. Collomb and C. Duboc, *Inorg. Chem.*, 2011, **50**, 10047–10055.
17 M. Ballesteros II and E. Y. Tsui, *Dalton Trans.*, 2020, **49**, 16305–16311.
18 F. Neese, *Wiley Interdiscip. Rev.: Comput. Mol. Sci.*, 2012, **2**, 73–78.
19 F. Neese, *Wiley Interdiscip. Rev.: Comput. Mol. Sci.*, 2025, **15**, e70019.
20 M. Garcia-Ratés and F. Neese, *J. Comput. Chem.*, 2019, **40**, 1816–1828.
21 M. Garcia-Ratés and F. Neese, *J. Comput. Chem.*, 2020, **41**, 922–939.
22 F. Neese, *J. Comput. Chem.*, 2023, **44**, 381–396.
23 P. Pracht, F. Bohle and S. Grimme, *Phys. Chem. Chem. Phys.*, 2020, **22**, 7169–7192.
24 S. Grimme, *J. Chem. Theory Comput.*, 2019, **15**, 2847–2862.
25 P. Pracht, S. Grimme, C. Bannwarth, F. Bohle, S. Ehlert, G. Feldmann, J. Gorges, M. Müller, T. Neudecker, C. Plett, S. Spicher, P. Steinbach, P. A. Wesołowski and F. Zeller, *J. Chem. Phys.*, 2024, **160**, 114110.
26 A. Hellweg and D. Rappoport, *Phys. Chem. Chem. Phys.*, 2015, **17**, 1010–1017.
27 D. Rappoport and F. Furche, *J. Chem. Phys.*, 2010, **133**, 134105.
28 A. V. Marenich, C. J. Cramer and D. G. Truhlar, *J. Phys. Chem. B*, 2009, **113**, 6378–6396.
29 M. Bursch, J.-M. Mewes, A. Hansen and S. Grimme, *Angew. Chem., Int. Ed.*, 2022, **61**, e202205735.
30 S. Grimme, F. Bohle, A. Hansen, P. Pracht, S. Spicher and M. Stahn, *J. Phys. Chem. A*, 2021, **125**, 4039–4054.
31 Y. Shinkai, Y. Ding, T. Matsui, G. Devitt, M. Akiyama, T.-L. Shen, M. Nishida, T. Ida, T. Akaike, S. Mahajan, J. M. Fukuto, Y. Shigeta and Y. Kumagai, *eLife*, 2025, **12**, RP92120.
32 A. B. Pangborn, M. A. Giardello, R. H. Grubbs, R. K. Rosen and F. J. Timmers, *Organometallics*, 1996, **15**, 1518–1520.
33 (*a*) CCDC 2521016: Experimental Crystal Structure Determination, 2026, DOI: 10.5517/ccdc.csd.cc2qmb3t; (*b*) CCDC 2521017: Experimental Crystal Structure Determination, 2026, DOI: 10.5517/ccdc.csd.cc2qmb4v; (*c*) CCDC 2521018: Experimental Crystal Structure Determination, 2026, DOI: 10.5517/ccdc.csd.cc2qmb5w; (*d*) CCDC 2521019: Experimental Crystal Structure Determination, 2026, DOI: 10.5517/ccdc.csd.cc2qmb6x; (*e*) CCDC 2521020: Experimental Crystal Structure Determination, 2026, DOI: 10.5517/ccdc.csd.cc2qmb7y.